Electronic Supplementary Material (ESI) for Journal of Materials Chemistry A.

Supporting information

One-Dimensional Channel Self-Standing MOF Cathode for Ultrahigh-Energy-Density Flexible Ni-Zn Batteries

Ping Man [+a,b,c], Bing He[+a,b,c,d], Qichong Zhang[e], Zhenyu Zhou[a,b], Chaowei Li [a,b,c], Qiulong Li[a,b], Lei Wei[e] and Yagang Yao* [a,b,d]

a. Division of Advanced Nanomaterials, Key Laboratory of Nanodevices and Applications, Joint Key Laboratory of Functional Nanomaterials and Devices, CAS Center for Excellence in Nanoscience, Suzhou Institute of Nano-tech and Nano-bionics, Chinese Academy of Sciences, Suzhou 215123, China

b. National Laboratory of Solid State Microstructures, College of Engineering and Applied Sciences, and Collaborative Innovation Center of Advanced Microstructures, Nanjing University, Nanjing 210093, China

c. School of Nano Technology and Nano Bionics, University of Science and Technology of China, Hefei, 230026, China

d. Division of Nanomaterials, Suzhou Institute of Nano-Tech and Nano-Bionics, Nanchang, Chinese Academy of Sciences, Nanchang 330200, China

e. School of Electrical and Electronic Engineering, Nanyang Technological University, 50 Nanyang Avenue, 639798, Singapore

[*] Corresponding author: Email: ygyao2018@nju.edu.cn.

[+] These authors contribute equally to this work.

1. Materials Characterizations

The morphologies and microstructures of the electrodes and accordingly powder were examined by Scanning Electron Microscope (SEM, Hitachi S-4800, 5 KV). Transmission electron microscopy (TEM) images, corresponding element mapping analysis and energy-dispersive spectroscopy (EDS) were measured by a high-resolution transmission electron microscope (FEI Tecnai G2 20). The crystal structure and chemical composition of samples were characterized by X-ray diffraction (XRD, Rigaku D/MAX2500 V) and X-ray photoelectron spectrometer (XPS, ESCALab MKII).

2. Electrochemical Performance Measurements

The electrochemical characterizations of single electrode was analyzed by cyclic voltammetry curves and galvanostatic charge/discharge curves measured on an electrochemical workstation (CHI 760E, Chenhua). Electrochemical impedance spectroscopy (EIS) measurements on an Autolab system (Metroohm PGSTAT302N). For three electrode system tests, pure CNTF, Ni-MOF-74@CNTF, Ni-MOF-74 powder, NiO_x@CNTF, and Zn wire electrodes were directly used as the working electrode, Ag/AgCl and Pt wire were used as the reference electrode and the counter electrode, respectively, 2 M KOH was used as the aqueous electrolyte. The aqueous Ni-Zn battery was assembled using Ni-MOF-74@CNTF, Zn wire, and ZnO saturated 2 M KOH solution as the cathode, anode, and electrolyte, respectively. For the flexible Zn-Ni full cell, the Ni-MOF-74@CNTF and Zn wire were used as the cathode and anode, respectively, with the KOH–PVA as the gel electrolyte. For comparison, the Ni-MOF-74 powder electrode was made by putting the mixture of 70% Ni-MOF-74 powder, 20% acetylene black, and 10% polytetrafluoroethylene with N-Methyl pyrrolidone as solvent on the carbon cloth, with the same loading mass of 0.4 mg cm^{-1} of binder-free Ni-MOF-74@CNTF electrode. Finally, it was dried at 60^oC in vacuum overnight to obtain the powder electrodes.

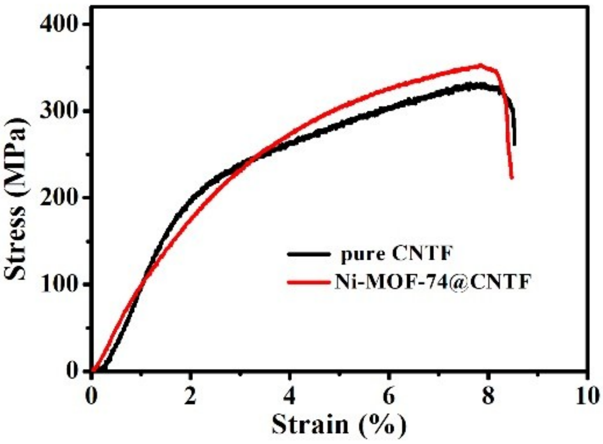

Figure S1 Typical stress–strain curves of pure CNTF and Ni-MOF-74@CNTF.

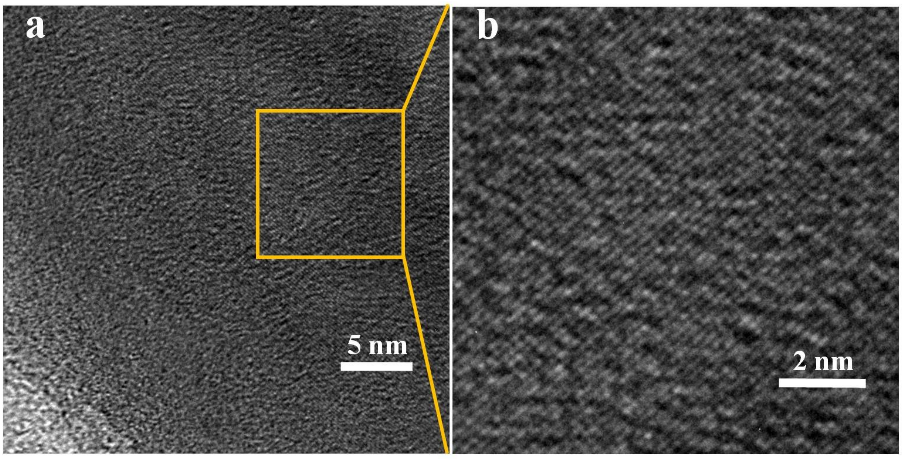

Figure S2 HRTEM images of the prepared Ni-MOF-74 sample.

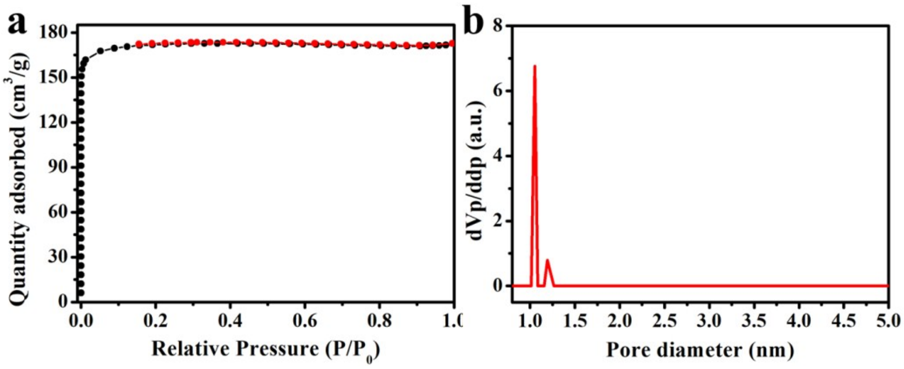

Figure S3 (a) N_2 adsorption-desorption isotherms of Ni-MOF-74, and (b) pore distribution of Ni-MOF-74.

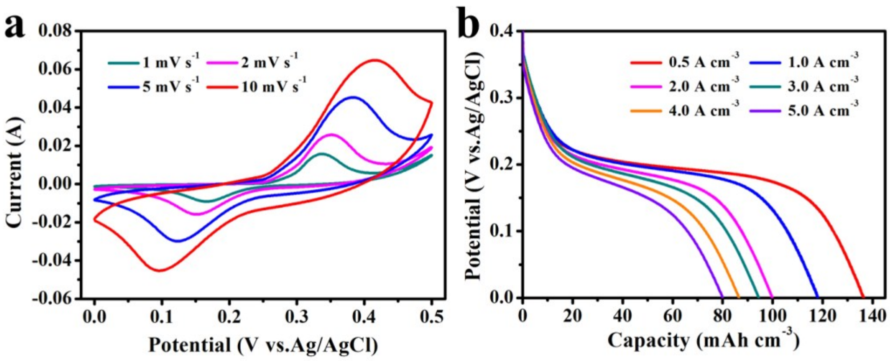

Figure S4 Electrochemical performance of Ni-MOF-74 powder electrodes. (a) CV curves at the scan rates from 1 to 10 mV s^{-1}. (b) GCD curves of at current densities from 0.5 to 5.0 A cm^{-3}.

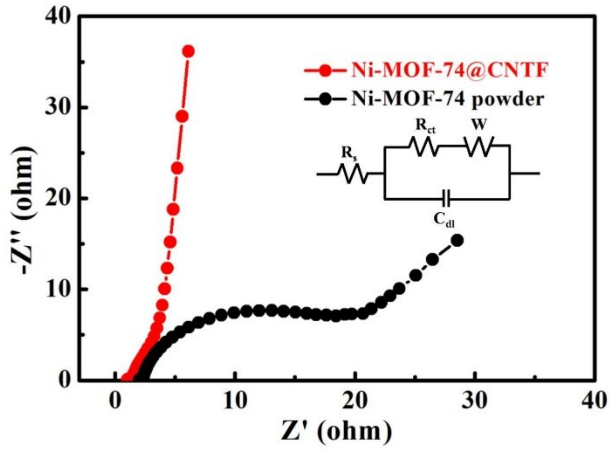

Figure S5 The equivalent circuit of electrochemical impedance spectrum of Ni-MOF-74@CNTF and Ni-MOF-74 powder electrode.

The equivalent circuit consists of series resistance (R_s), charge transfer resistance (R_{ct}), double layer capacitance (C_{dl}) and Warburg behavior (W). R_s represents the total resistance of the electrolyte and electrical contacts, estimated by a real axis intercept. R_{ct} is the faradic charge-transfer resistance at the interface between the electrode and the electrolyte, which is related to the semicircle diameter in the plot. A small semicircle diameter in the high frequency region and a large slope in the low frequency region indicate a small charge-transfer resistance and a fast ion-diffusion rate, respectively. For the binder-free Ni-MOF-74@CNTF electrode, the fitting values of R_s and R_{ct} are 1.84 Ω and 2.69 Ω, respectively. Compared to the values of R_s (3.4 Ω) and R_{ct} (23.36 Ω) for the Ni-MOF-74 powder electrode, the self-standing Ni-MOF-74@CNTF electrode shows better electron and ionic conductivity.

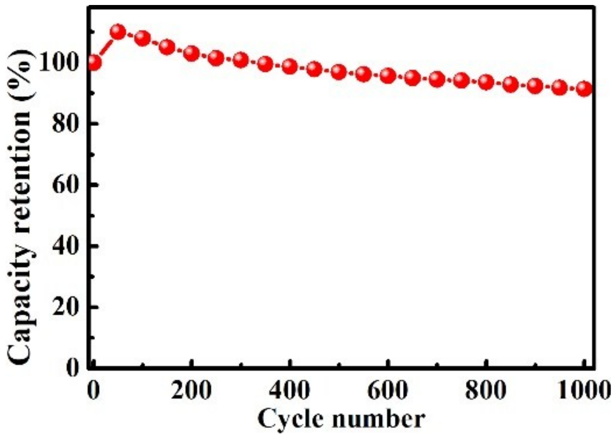

Figure S6 Cycling tests of the binder-free Ni-MOF-74@CNTF electrode.

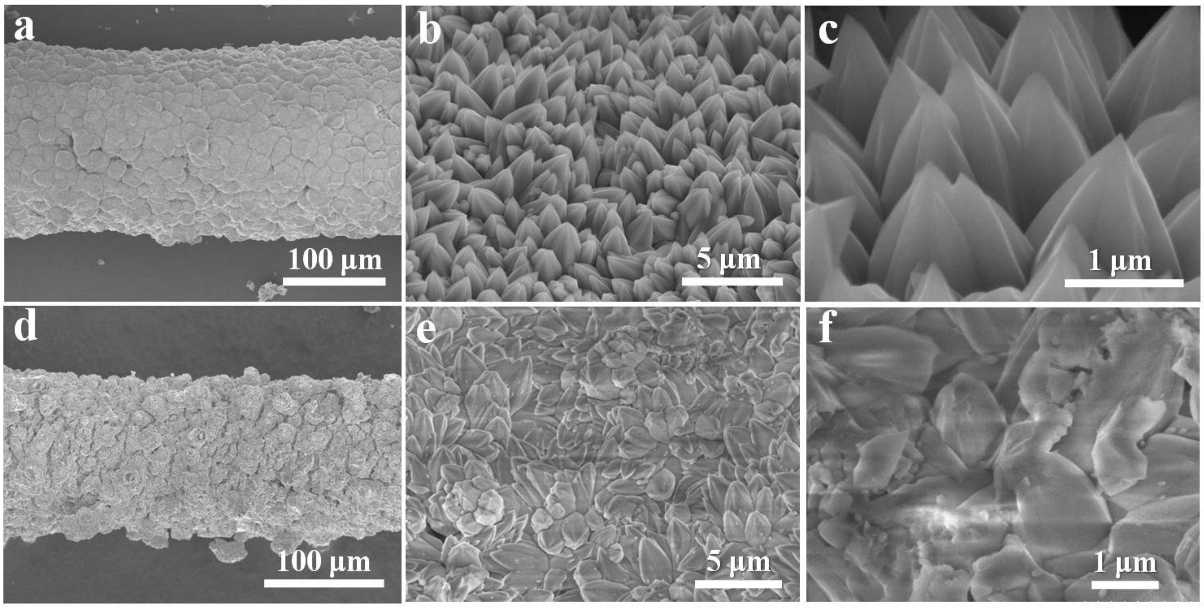

Figure S7 The SEM images of Ni-MOF-74@CNTF electrode (a-c) before and (d-f) after cycle test at increasing magnification.

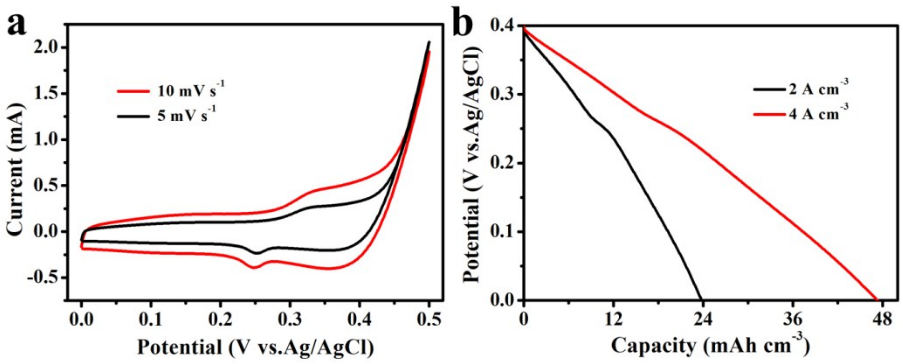

Figure S8 (a) CV and (b) GCD of NiO@CNTF electrode under same test condition.

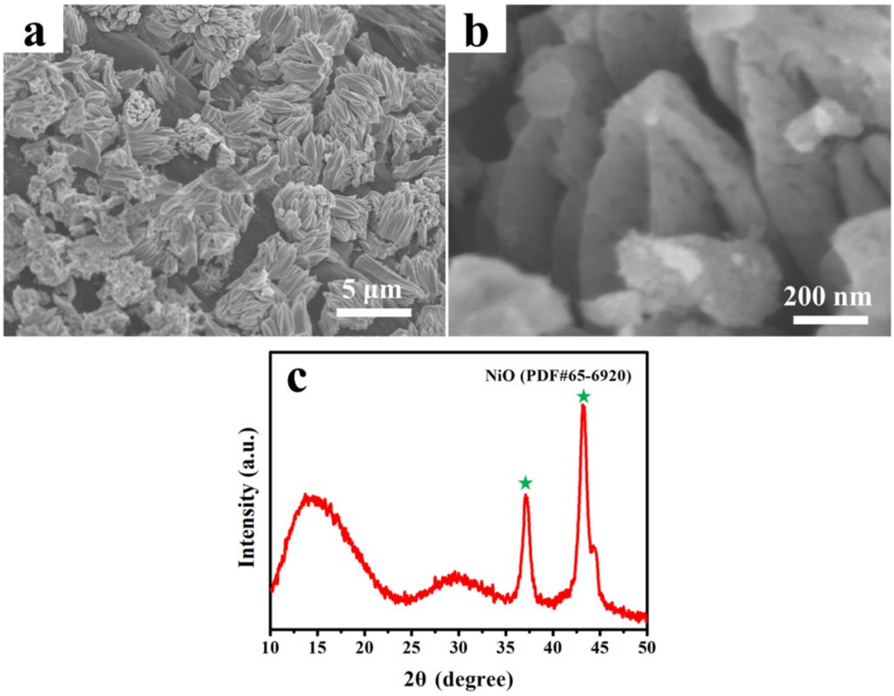

Figure S9 (a-b) SEM images with different resolutions, (b) XRD pattern of NiO@CNTF annealed by Ni-MOF-74@CNTF.

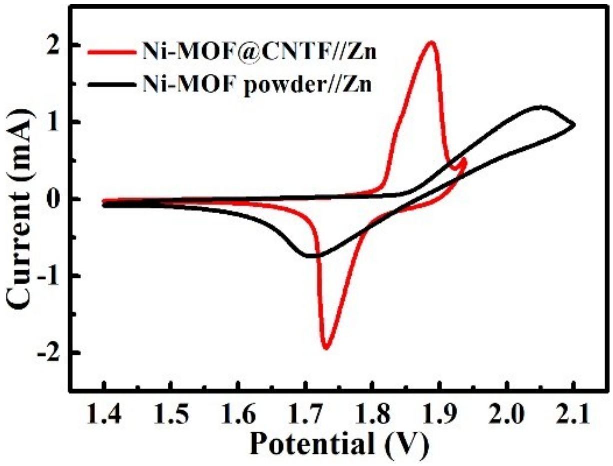

Figure S10 CV curves of aqueous Ni-MOF-74//Zn and Ni-MOF-74 powder//Zn battery at the scan rate of 1 mV s^{-1}.

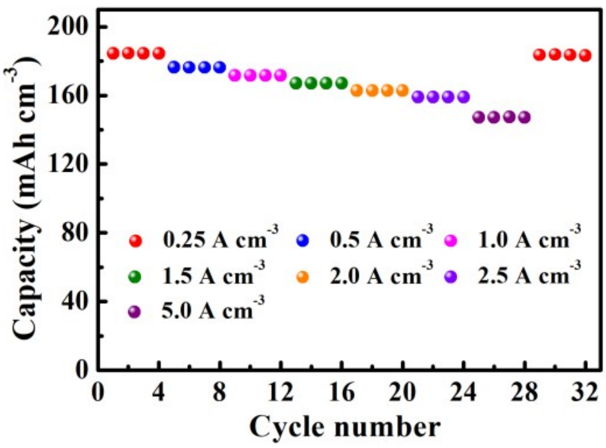

Figure S11 Rate performance of aqueous Ni-MOF-74//Zn battery.

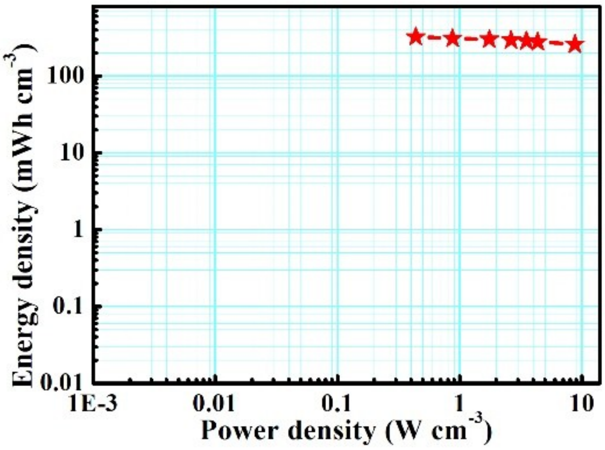

Figure S12 Energy and powder density of aqueous Ni-MOF-74//Zn battery.

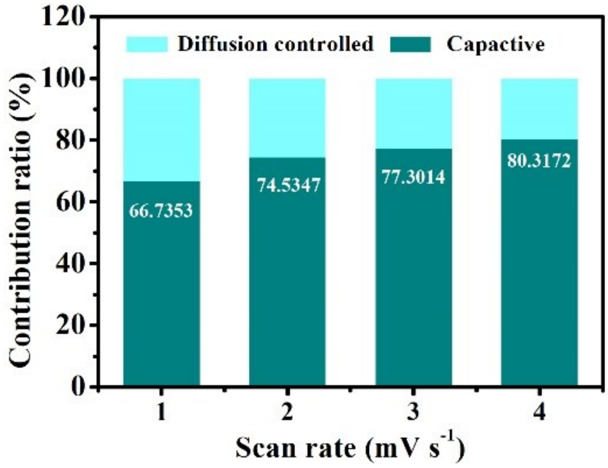

Figure S13 Bar chart pf the percent of capacity contribution at different scan rates of the quasi-solid-state FANZB.

Table S1 Comparison of Ni-MOF-74@CNTF with reported Ni-Zn batteries

Device	Shape	$V_{discharge}$(V)	C	Rate	E	P	Ref.
Ni-MOF-74//Zn	**Fiber-shaped**	**~1.75**	**1808.5 mAh cm^{-3}**	**80% (20)**	**186.28 mWh cm^{-3}**	**8.4 W cm^{-3}**	**Our work**
NiO // ZnO	planar-shaped	~1.77	0.39 mAh cm^{-2}	~59.2% (20)	7.76 mWh cm^{-3}	0.54 W cm^{-3}	1
Ni–NiO//Zn	Fiber-Shaped	1.7–1.8	116.1 µAh cm^{-3}	38.4% (10)	0.67 mWh cm^{-3}	0.22 W cm^{-3}	2
Ni//Zn@Li-RTiO$_2$	Fiber-shaped	1.7			0.034 Wh cm^{-3}	2.4 W cm^{-3}	3
NiCo//Zn	Fiber-shaped	~1.6	18.7 mAh cm^{-3}	8.02% (80)	8.0 mWh cm^{-3}	2.2 W cm^{-3}	4
Ni@Ni(OH)$_2$//Zn	planar-shaped	~1.75	150.1 µAh cm^{-2}	59.2% (20)	0.12 W h cm^{-3}	15.8 W cm^{-3}	5
NNA@Zn	planar-shaped	~1.73	247 mAh g^{-1}	85% (8)	0.057 mWh cm^{-2}	2.17 mW cm^{-2}	6
Ni(OH)$_2$//Zn	planar-shaped	~1.75	383 mAh g^{-1}	27.1% (4.5)	2.9 m Wh cm^{-3}	136.4 mW cm^{-3}	7
SANF//Zn	planar-shaped	1.73	0.422 mAh cm^{-2}	26.8% (3.75)	15.1 mW h cm^{-3}	278 mW cm^{-3}	8
HD-NiS$_2$/rGO-5 //Zn	planar-shaped	1.75	134.7 mAh cm^{-3}		18.7 m Wh cm^{-3}		9

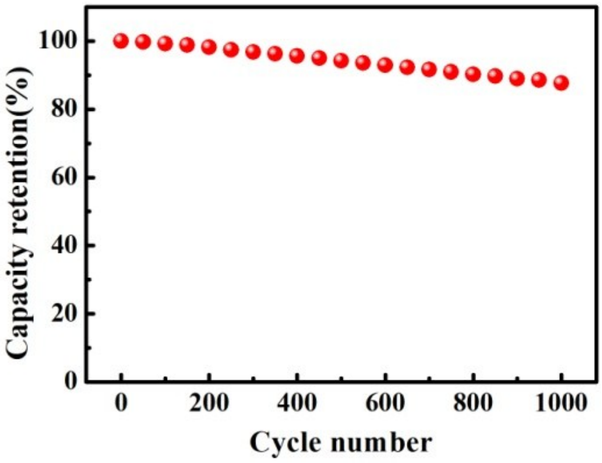

Figure S14 Cycle stability of the quasi-solid-state FANZB.

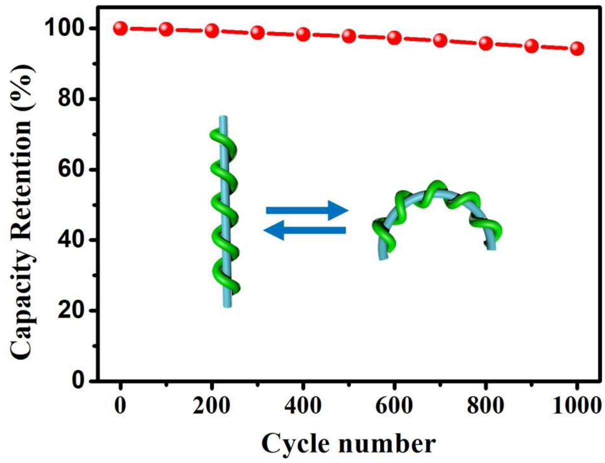

Figure S15 Normalized capacities of our device bent 90° for 1000 cycles.

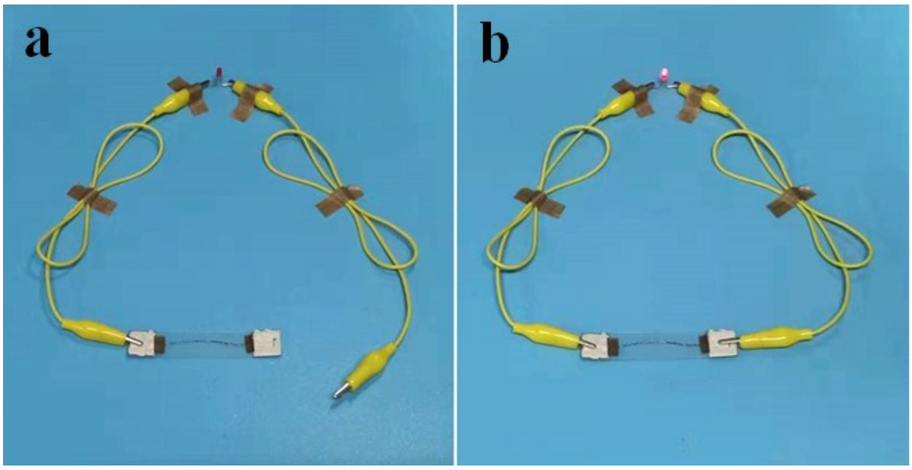

Figure S16 A LED powered by the FANZB device.

Reference

[1] J. Liu, C. Guan, C. Zhou, Z. Fan, Q. Ke, G. Zhang, C. Liu and J. Wang, *Adv. Mater.*, 2016, **28**, 8732-8739.

[2] Y. Zeng, Y. Meng, Z. Lai, X. Zhang, M. Yu, P. Fang, M. Wu, Y. Tong and X. Lu, *Adv. Mater.*, 2017, **29**, 1702698.

[3] P. Li, Z. Jin and D. Xiao, *Energy Storage Mater.*, 2018, **12**, 232-240.

[4] H. Zhang, X. Zhang, H. Li, Y. Zhang, Y. Zeng, Y. Tong, P. Zhang and X. Lu, *Green Energy & Environment*, 2018, **3**, 56-62.

[5] Z. Hao, L. Xu, Q. Liu, W. Yang, X. Liao, J. Meng, X. Hong, L. He and L. Mai, *Adv. Funct. Mater.*, 2019, **29**, 1808470.

[6] C. Xu, J. Liao, C. Yang, R. Wang, D. Wu, P. Zou, Z. Lin, B. Li, F. Kang and C.-P. Wong, *Nano Energy*, 2016, **30**, 900-908.

[7] J. Li, M. K. Aslam and C. Chen, *J. Electrochem. Soc.*, 2018, **165**, A910-A917.

[8] R. Wang, Y. Han, Z. Wang, J. Jiang, Y. Tong and X. Lu, *Adv. Funct. Mater.*, 2018, **28**, 1802157.

[9] W. Shi, J. Mao, X. Xu, W. Liu, L. Zhang, X. Cao and X. Lu, *J. Mater. Chem. A*, 2019, **7**, 15654-15661.